ASTROBIOLOGY
Volume 18, Number 8, 2018

DOI: 10.1089/ast.2017.1685

Characterization of Microbial Communities Hosted in Quartzofeldspathic and Serpentinite Lithologies in Jeffrey Mine, Canada

Jennifer Ronholm,[1,2] Jacqueline Goordial,[3,*] Haley M. Sapers,[3,4,†,‡,§] Matthew R.M. Izawa,[5,**] Daniel M. Applin,[5] Alexandra Pontefract,[6] Christopher R. Omelon,[7] Guillaume Lamarche-Gagnon,[3,††] Edward A. Cloutis,[5] and Lyle G. Whyte[3]

Abstract

The microbial ecology and activity of serpentine deposits and associated hydrated minerals are largely unknown. Previous research has largely focused on microbial communities in active serpentinizing systems, whereas relatively little research has demonstrated the ability of serpentine deposits to host microbial communities after the cessation of serpentinization. Given the potential role of serpentinization reactions fueling primitive microbial metabolisms on early Earth and the identification of serpentine deposits on Mars, knowledge of these geobiological relationships and potential for serpentine to host extant microbial communities and preserve biosignatures is increasingly important for planetary exploration seeking signs of life. The selection of habitable sites most likely to yield putative biosignatures is crucial to mission success. In this study, we aimed to characterize, on the basis of both metabolic activity and taxonomic composition, the microbial communities hosted in two naturally co-occurring and mineralogically distinct substrates within the serpentine-rich Jeffrey Mine pit–igneous quartzofeldspathic intrusives and serpentinite. Detection of heterotrophic activity in both lithologies at 24°C, and in serpentinite at −5°C, demonstrated that each substrate had the ability to host a viable microbial community, at Mars-relevant temperatures. Targeted amplicon sequencing subsequently showed the presence of bacterial, fungal, and photosynthetic microbial communities in both substrates. Here, we have demonstrated the presence of a viable lithic microbial community within two rock types in the Jeffrey Mine and provided evidence that lithologies associated with serpentine deposits and proximal hydrated minerals have the ability to support diverse prokaryotic and eukaryotic microbial colonization.Key Words: Asbestos—Astrobiology—Serpentinite—Geobiology—Quartzofeldspathic—Mars. Astrobiology 18, 1008–1022.

Departments of [1]Food Science and Agricultural Chemistry, [2]Animal Science, and [3]Department of Natural Resource Science, Faculty of Agricultural and Environmental Sciences, McGill University, Ste Anne de Bellevue, Canada.
[4]Department of Earth and Planetary Sciences, Centre for Planetary Science and Exploration, University of Western Ontario, London, Canada.
[5]Department of Geography, University of Winnipeg, Winnipeg, Canada.
[6]Department of Earth, Atmospheric, and Planetary Sciences, Massachusetts Institute of Technology, Cambridge, Massachusetts.
[7]Department of Geology, The University of Kansas, Lawrence, Kansas.
*Present address: Bigelow Laboratory for Ocean Sciences, 60 Bigelow Drive, East Boothbay, ME 04544.
†Present address: Division of Geological and Planetary Sciences, California Institute of Technology, 1200 East California Boulevard, Pasadena, CA 91125.
‡Present address: Astrobiology and Planetary Chemistry Group, Science Division, NASA Jet Propulsion Laboratory, 4800 Oak Grove Drive, Pasadena, CA 91101.
§Present address: Department of Earth Sciences, Dornsife College of Letters, Arts, and Sciences, University of Southern California, University Park Campus, Los Angeles, CA 900007.
**Present address: Institute for Planetary Materials, Okayama University–Misasa, 827 Yamada, Misasa, Tottori 682-0193, Japan.
††Present address: School of Geographical Sciences, University of Bristol, Bristol BS8 1SS, United Kingdom.

1. Introduction

LITHIC MICROBIAL COMMUNITIES—organisms living in close association with rocks—occupy one of the most ubiquitous niches on Earth, even persisting in extreme environments. They have been investigated in several environments including the Rocky Mountains (Walker and Pace, 2007a), hot (Davila *et al.*, 2008; Stivaletta and Barbieri, 2009; Stivaletta *et al.*, 2010; Caruso *et al.*, 2011; Wierzchos *et al.*, 2011) and cold deserts (Omelon *et al.*, 2006, 2007; Wong *et al.*, 2009; Pointing *et al.*, 2010; Caruso *et al.*, 2011; Ziolkowski *et al.*, 2013; Goordial *et al.*, 2016), geothermal hot springs (Walker *et al.*, 2005), Arctic springs (Starke *et al.*, 2013), and the deep subsurface (Lee *et al.*, 2015; Orcutt *et al.*, 2015; Jørgensen and Zhao, 2016). Microbe–mineral interactions are an inherent feature of lithic microbial communities, with implications for both the microbe and the mineral. Microbes alter rocks through physical and chemical processes including weathering, metal cycling, and soil development (Walker *et al.*, 2005; Walker and Pace, 2007b). Given the sheer volume of lithic environments on Earth, these communities can affect element cycles and climate on a global scale (Walker and Pace, 2007b; Ziolkowski *et al.*, 2013). Conversely, the lithic microhabitat can protect microbes from solar radiation and desiccation, be a source of micronutrients, and provide a stable growth surface (Walker *et al.*, 2005; Wierzchos *et al.*, 2011). Owing to the intimate interaction of microbe and mineral, mineralogical properties of the rock likely have a role in the selection of microbial communities; however, few specific details of how this is accomplished are known (Walker and Pace, 2007b). Microbial mineral alterations can also result in the formation of geological biosignatures—a record of terrestrial life and a possible marker for extinct, or even extant, extraterrestrial life (Walker and Pace, 2007b).

Serpentine deposits are of significant astrobiological interest. Serpentine forms through the process of serpentenization through hydrothermal alteration of ultramafic rocks at temperatures up to 400°C (Evans, 2004). The presence of serpentine indicates the presence of a highly reducing and highly alkaline aqueous fluid. The process of serpentinization can produce hydrogen, an important energy source for chemoautolithic microrganisms (Schulte *et al.*, 2006). Hydrogen-based metabolisms are likely one of the most primitive, suggesting a role for serpentinization processes in the early evolution of life on earth. In the absence of microorganisms, the abiotic reaction of hydrogen with carbon dioxide will produce methane (Oze and Sharma, 2005). Methane is a source of energy in several bacterial metabolic reactions, provided there is oxygen available (Serrano-Silva *et al.*, 2014). Surface exposures of serpentine are indicative of either past episodes of active serpentinization and subsequent exhumation through tectonic processes or active serpintinization at depth and exposure through a combination of tectonic and/or erosional processes. Surficial serpentine deposits identified on Mars using Mars Reconnaissance Orbiter data in Noachian terranes suggest that the processes forming these deposits could have resulted in hydrogen-rich aqueous habitats capable of supporting microbial life (Ehlmann *et al.*, 2010).

The Jeffrey Mine (Fig. 1A) is an open-pit chrysotile asbestos mine hosted in the Early Ordovician ophiolite belt of the Quebéc Appalachians that has undergone two serpentinization events (Laurent and Hébert, 1979). Quartzofeldspathic

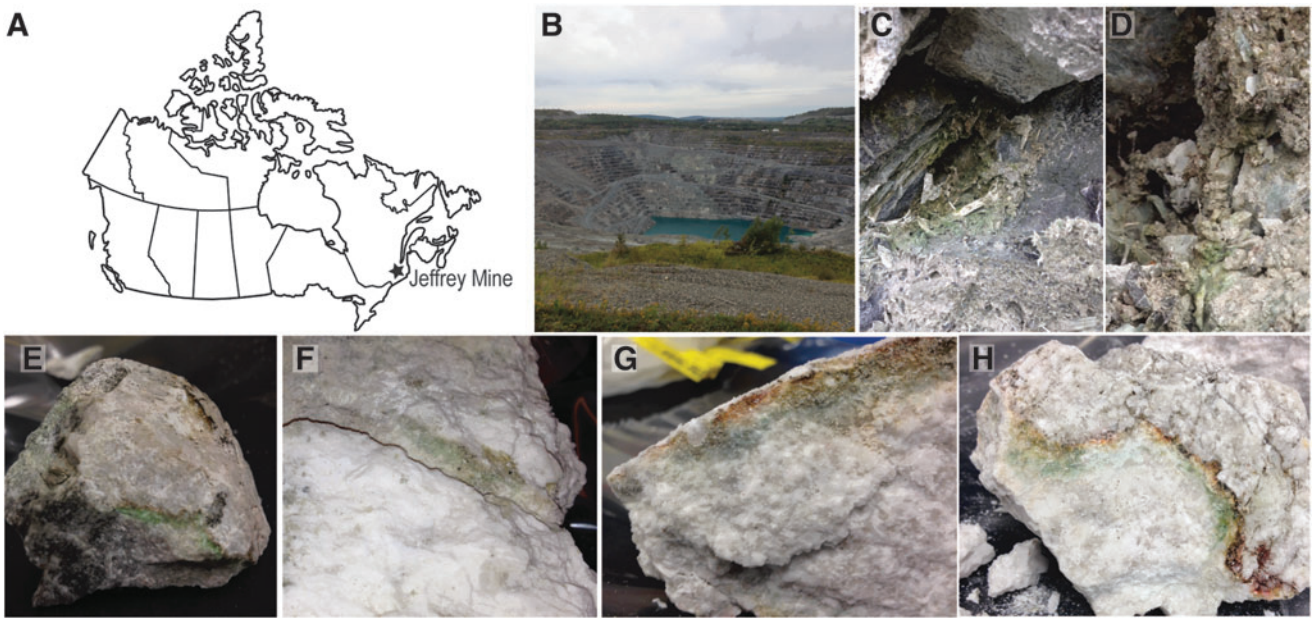

FIG. 1. Study site location and sample collection. **(A)** Samples were collected from the Jeffrey Mine located in Asbestos, Quebéc, Canada. **(B)** The Jeffrey Mine is an open pit mine that is not currently active. Samples collected included **(C)** ASB-J06 friable serpentinite, **(D)** ASB-J07 small colonized serpentinite rocks, and **(E–H)** four quartzofeldspathic endoliths. The **(E)** ASB-J01 and **(F)** ASB-J02 endoliths were green, whereas endoliths **(G)** ASB-J04 and **(H)** ASB-J05 were layered, and consisted of red, orange, yellow, and green bands. The field view for each image is approximately: **(B)** 500 m, **(C)** 15 cm, **(D)** 10 cm, **(E)** 10 cm, **(F)** 3 cm, **(G)** 2 cm, and **(H)** 5 cm.

intrusives including granitic to granodioritic rocks are present and likely formed during the late stages of ophiolite formation on the Laurentian margin during the Taconic (~470–460 Ma) orogeny (Normand and Williams-Jones, 2007). Today, the main rock type present in the mine is serpentinite, with lesser amounts of carbonate. The excellent surficial exposures of serpentine at the Jeffrey Mine render it an interesting analogue for serpentine deposits on Mars (Ehlmann *et al.*, 2010; Qadi *et al.*, 2015).

Putative detections of methane in the atmosphere of Mars have been spatially linked to surfaces with spectral properties consistent with abundant serpentine-group minerals (Blamey *et al.*, 2015). Although this is a controversial correlation, it is unclear whether this methane is produced abioitically through the reaction of H_2 as a by-product of active subsurface serpentinization with abundant CO_2, but the possibility exists that subsurface active serpentinization is producing H_2 utilized by a subsurface microbial community producing methane through methanogenesis. Indeed, recent studies have demonstrated active methanogenic and methanotropic microbial communities in ground water associated with serpentinite deposits (Brazelton *et al.*, 2017), although bacterial diversity is limited (Twing *et al.*, 2017). This study was undertaken to investigate the ability of surficial serpentinite lithologies, as well as proximal lithologies, to host active microbial communities after the cessation of active serpentinization. Serpentinites are important targets for Mars exploration because they are indicators of hydrothermal/aqueous alteration, associated with hydrogen and methane production, and possibly abiotic hydrocarbon generation on Earth (Lang *et al.*, 2012) and possibly early Mars (Quesnel *et al.*, 2009; Marlow *et al.*, 2014). Serpentinites are found in or near a number of Mars 2020 and ExoMars rover landing sites (Ehlmann *et al.*, 2010; Wray and Ehlmann, 2011; Ehlmann and Mustard, 2012), and it is important to understand the ability of surficial sepentinites to host active microbial communities.

2. Materials and Methods

2.1. Site description and sample collection

All mineralogical samples were aseptically collected and placed into sterile bags on October 16, 2013, from the Jeffery Mine located in Asbestos, Quebéc, Canada (Fig. 1A, B). Samples were differently collected based on lithology. Quartzofeldspathic samples were chipped away in large pieces from rock faces using a rock hammer. Serpentinite samples were softer and were scraped from the surface also using a rock hammer. Two samples of serpentinite (ABS-J06 and ABS-J07) were collected from the north face of the mine (Fig. 1C, D). A total of four colonized quartzofeldspathic intrusive rocks, which included samples ABS-J01 and ABS-J02 (Fig. 1E, F) collected from the north side of the mine, and samples ABS-J04 and ABS-J05 (Fig. 1G, H) were collected from the south wall of the mine. After collection, samples were immediately placed on ice then stored at −20°C until use. Subsamples were taken from the original for each of the subsequent experiments and treated as outlined hereunder.

2.2. X-ray diffraction

X-ray diffraction (XRD) data were collected in continuous scan mode from 5° to 80° 2θ with a Bruker D8 Advance DaVinci automated powder diffractometer. Full settings and protocols can be found in the Supplementary Materials and Methods section (Supplementary Data are available online at www.liebertonline.com/ast).

2.3. Spectroscopy

Ultraviolet-visible-near infrared (IR; 350–2500 nm) and mid-IR (2–25 μm) reflectance spectroscopy as well as Raman spectroscopy was performed on each of the samples. Full settings and protocols can be found in the Supplementary Materials and Methods section.

2.4. ^{14}C acetic acid heterotrophic activity assays

Individual microcosms were created in sealed glass containers and composed of either 10 g of crushed quartzofeldspathic (homogenized mixture of four collected samples) or 2 g of crushed and homogenized serpentinite (Steven *et al.*, 2007). Experiments were carried out as outlined in Goordial *et al.* (2016). In brief, each microcosm was performed in triplicate and included duplicate sterilized controls (dry autoclaved twice for 2 h at 120°C and 1.0 atm, with a 24 h period between autoclaving). Microcosms were spiked with 0.045 mCi/mL (~100,000 disintegrations per minute) of ^{14}C acetic acid. Cold acetic acid was added to a final concentration of 15 mM acetic acid, as well as double distilled and sterilized H_2O (50 μL) added to each microcosm. A CO_2 trap was used to capture metabolized ^{14}C acetic acid before quantification that consisted of 0.5 mL 1 M KOH in a glass vial placed inside the microcosm. The microcosms were incubated at either 22°C or −5°C for 18 weeks. Measurements of radioactivity were determined by liquid scintillation spectrometry on an LS 6500 Multi-purpose Scintillation Counter (Beckman Coulter, CA) once a week for samples incubated at 22°C and once every 2 weeks for samples incubated at −5°C.

2.5. Imaging

High-resolution imaging of the serpentinite samples was conducted at the Western University Nanofabrication Facility. Samples were mechanically crushed using a mortar and pestle into ~1 mm fragments under sterile conditions, and a standard preparation protocol was used to prepare biological samples for scanning electron microscopy under high-vacuum conditions (Hayat, 2000). In brief, samples were fixed in 2% glutaraldehyde overnight at room temperature. After fixation, samples were ethanol dehydrated by subsequent 15 min immersions in increasing concentrations of ethanol (50%, 75%, and 100%) followed by a final submersion in 100% ethanol (Hayat, 2000). The dehydrated samples were critical point dried to preserve cell structure. Samples were then manually transferred to standard titanium electron microscopy imaging stubs using a binocular microscope. A combination of carbon tape and silver paint was used to affix samples to the titanium stubs to allow the dissipation of charge buildup. Each sample was plasma coated with 10 nm of amorphous osmium using a Filgen OPC80T Osmium Plasma Coater with an OsO_4 source. High-resolution imaging was carried out under high vacuum on a LEO (Zeiss, Oberkochen, Germany) 1540XB FIB/SEM under an accelerating voltage of 1 kV and a working distance of 3.8 mm.

Quartzofeldspathic samples were prepared for scanning electron microscopy (SEM) imaging in secondary electron mode by isolating small pieces of colonized rock by

mechanical chiseling, then fixing the pieces in 2.5% glutaraldehyde overnight. Rocks were dehydrated using graded ethanol series (70%, 90%, 95%, and 100%) and critical point dried using a Samdri 790 (Tousimis Research Group). Samples were subsequently platinum coated and imaged on a LEO (Zeiss) Supra 40 field emission scanning electron microscope in secondary electron mode.

2.6. DNA purification and targeted amplicon sequencing

Total DNA was extracted from each sample using the UltraClean Soil DNA Kit (MoBio, CA). Partial 16S rRNA gene (bacteria), internal transcribed spacer (ITS) (fungi), and 23 large subunit (LSU) plastid rRNA (photosynthetic bacterial/algae) amplicons were produced for each sample. Partial bacterial 16S rRNA gene amplicons were produced using the primers 27F (5′-AGRGTTTGATCMTGGCTCAG-3′) and Gray519r (5′-GTNTTACNGCGGCKGCTG-3′), which target the V1–V3 hypervariable regions as in McFrederick *et al.* (2013). Partial fungal ITS amplicons were produced using the primer pair ITS1F (5′-CTTGGTCATTTAGAGGAAG TAA-3′) and ITS2 (5′-GCTGCGTTCTTCATCGATGC-3′) as outlined in Bell *et al.* (2013). Partial bacterial/algal 23S rRNA amplicons were produced using the forward primer (5′-GGACAGAAAGACCCTATGAA-3′) and reverse primer (5′-TCAGCCTGTTATCCCTAGAG-3′) that flank the V domain of the 23S plastid rRNA gene, only present in cyanobacteria and algal plastids (Sherwood and Presting, 2007). An attempt was also made to amplify the 16S rRNA gene from archaea using the forward primer 349F (5′-GYGCASCAGKCGMGA AW-3′) and reverse primer 806R (5′-GGACTACVSGG GTATCTAAT-3′) (Swan, 2010); although several amplification parameters were tested, this primer pair was unable to produce an amplicon. Each sample was amplified using unique multiplex identifier (MID) tags from the extended MID set recommended by Roche Diagnostics.

Then 454 pyrosequencing was performed by Genome Quebec using the GS FLX Titanium platform (Roche, CT). Sequences were analyzed and classified using Mothur (Schloss *et al.*, 2011). Using Mothur (Schloss *et al.*, 2009), original .sff files for bacterial sequences were separated into .fasta and .qual files and trimmed using the flowgrams using ''sff.multiple'' with the following parameters: pdiffs = 5, bdiffs = 2, order = B, maxhomop = 8, minflows = 250, maxflows = 720, flip = T. Sequences were reduced to only unique sequences using ''unique.seqs'' and aligned to the Mothur-interpreted Silva bacterial database (April 22, 2012 version) with the ''align.seqs'' command. Aligned sequences were reduced to only the overlapping region using ''screen.seqs'' and ''filter.seqs'' (vertical = T, trump = .). Sequences were again reduced to only unique sequences using ''unique.seqs'' then preclustered into operational taxonomic units (OTUs) consisting of two or fewer different base pairs (bp) using the ''pre.cluster'' command (diffs = 2). Chimeras were removed using the uchime program within Mothur. A distance matrix was generated with ''dist.seqs'' (cutoff = 0.15) and OTUs were formed based on this distance matrix using ''cluster.'' All bacterial sequences were classified using the Silva bacterial database already mentioned using ''classify.seqs'' and the Wang method.

Prealignment steps for fungal ITS sequences were as described previously, until the alignment step. Unaligned sequences were chopped with ''chop.seqs'' with the parameters numbases = 249 and keep = front. Classification of ITS sequences was performed in Mothur using ''classify.seqs'' and the Wang method using the UNITE/QIIME 12_11 ITS reference database (alpha release, accessed April 2013).

Bacteria/Algal LSU sequences were also processed as described until the alignment step. Sequences were aligned to the Silva LSU bacterial database (accessed June 2014) with ''align.seqs.'' Sequences were then processed using the same steps outlined for the bacterial sequences until after the ''cluster'' command. At this step, the ''get.oturep'' command was used to retrieve a representative sequence for each OTU. Representative plastid sequences were classified using the MEGAN5 software (v. 5.3.0) (Huson, Auch, Qi, and Schuster, 2007) after BLASTn searches (Mount, 2007) against the GenBank nt database (www.ncbi.nlm.nih.gov/GenBank) (accessed June 2014) with default settings, and by excluding noncultured/environmental sequences from the target database. For MEGAN5 classification, lowest common ancestor (LCA) parameters were changed from default as to favor the taxonomic information of the best BLASTn hits to be assigned to a given read; LCA parameters were set to ''Min Support: 2,'' ''Min Score: 100,'' ''Max Expected: 1.0×10^{-5},'' ''Top percent: 2,'' and ''Min complexity:0.''

The number of bp kept for analysis was optimized for each primer set and was 300 bp for bacteria, 330 bp for plastid, and 249 bp for ITS. In all samples, OTUs clustered at 97% similarity. To construct the taxonomic profiles at phylum and order levels (Fig. 4), singletons were removed from the data set. Singletons remained in the data set for the statistical analysis.

2.7. Statistical analysis

The total bacterial, fungal, and bacterial/algal community was subsampled to the number of sequences in the smallest sample, using the ''make.shared'' command, followed by the ''sub.sample'' command where size equaled 1193 for bacteria, 523 for fungi, and 1074 for plastid rRNA. The ''collect.single'' command was used to calculate Good's coverage ($C = 1 - n/N$), and this value was multiplied by 100 to express the coverage of the library as a percentage, where n is the number singletons and N is the total number of sequences analyzed (Good, 1953). The ''collect.single'' command was also used to calculate the Chao and Inverted Simpson diversity indices.

3. Results

3.1. XRD analysis

Results of XRD analysis with the minerals identified from each sample are listed in Table 1. Quartzofeldspathic intrusive samples ASB-J01 and ASB-J02 are dominated by microcline feldspar, with some variation in the minor mineral phases present. Quartzofeldspathic intrusive samples ASB-J04 and ASB-J05 (Fig. 2) are hosted in a quartz/albite matrix with minor traces of microcline. The serpentinite samples are dominated by antigorite, with traces of clinochlore, chrysotile, and biotite (Table 1 and Fig. 2).

3.2. Reflectance spectra at 0.35–2.5 μm

Figure 3 shows reflectance and Raman spectra of the samples that demonstrate their spectral diversity and detectability

Table 1. Sample Descriptions (of Whole Rock or of Areas Individually Characterized) and X-Ray Diffraction Mineral Identifications

Sample	*Description*	*Major minerals*	*Minor minerals*
ASB-J01a	Quartzofeldspathic, bulk sample	Quartz	Tr. afghanite; tr. birnessite
ASB-J01b	Quartzofeldspathic, exterior of sample	Quartz	Tr. birnessite
ASB-J01c	Quartzofeldspathic, orange interior	Quartz	Tr. afghanite
ASB-J01d	Quartzofeldspathic, white interior	Quartz	Tr. dolomite
ASB-J01e	Quartzofeldspathic, chip with green endolith layer	Diopside, albite, microcline	Grossular, prehnite, biotite
ASB-J02a	Quartzofeldspathic, white with small endolith	Microcline	Prehnite, albite, sericite
ASB-J02b	Quartzofeldspathic, serpentinite spot	Antigorite, lizardite	
ADB-J04a	Quartzofeldspathic, red-brown (endolith?) spot	Quartz, albite	Microcline
ASB-J04b	Quartzofeldspathic, white endolith-free spot	Quartz, albite	Microcline
ASB-J04c	Quartzofeldspathic, green (endolith?) spot	Quartz, albite	Microcline
ASB-J05	Quartzofeldspathic, white with orange endoliths	Quartz, albite	Microcline
ASB-J06	Serpentinite, tabular, light green serpentinite	Antigorite	Clinchlore, chrysotile, biotite
ASB-J07	Serpentinite, serpentine+green endolith spots	Antigorite	Clinchlore

of organic absorption bands. Figure 3A shows five (labeled a–e) subsamples of ASB-J01. Despite visual identification of possible endoliths (Fig. 1) in ASB-J01c and e, there is no spectral evidence of chlorophyll—its strongest absorption band is located near 0.67 μm—nor carotenoids, whose strongest absorption bands are located in the 0.4–0.5 μm region. The reflectance spectra show differences in the visible region that correlate with their observed colors. The ASB-J01a–d spectra show only weak absorption bands in the 1.4 and 1.9 μm regions that are nondiagnostic and

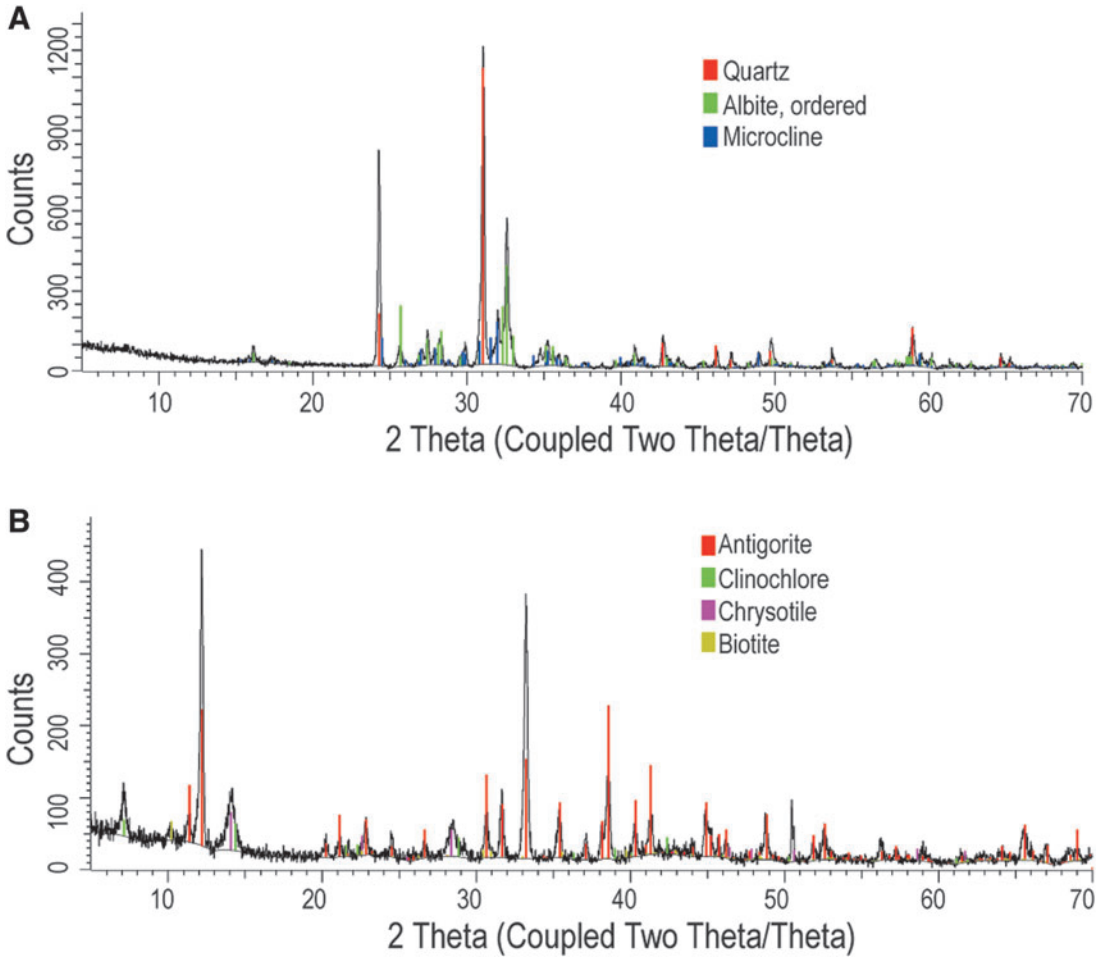

FIG. 2. Mineral identification and characterization. Each sample was analyzed by XRD and a summary is found in Table 1. A representative XRD pattern for both a quartzofeldspathic intrusive and serpentinite is shown here. The **(A)** quartzofeldspathic intrusive sample ASB-J04 is dominated by quartz and albite with minor amounts of microcline. **(B)** The major component of serpentinite sample ASB-J06 is antigorite, with minor traces of clinochlore, chrysotile, and biotite. XRD, X-ray diffraction.

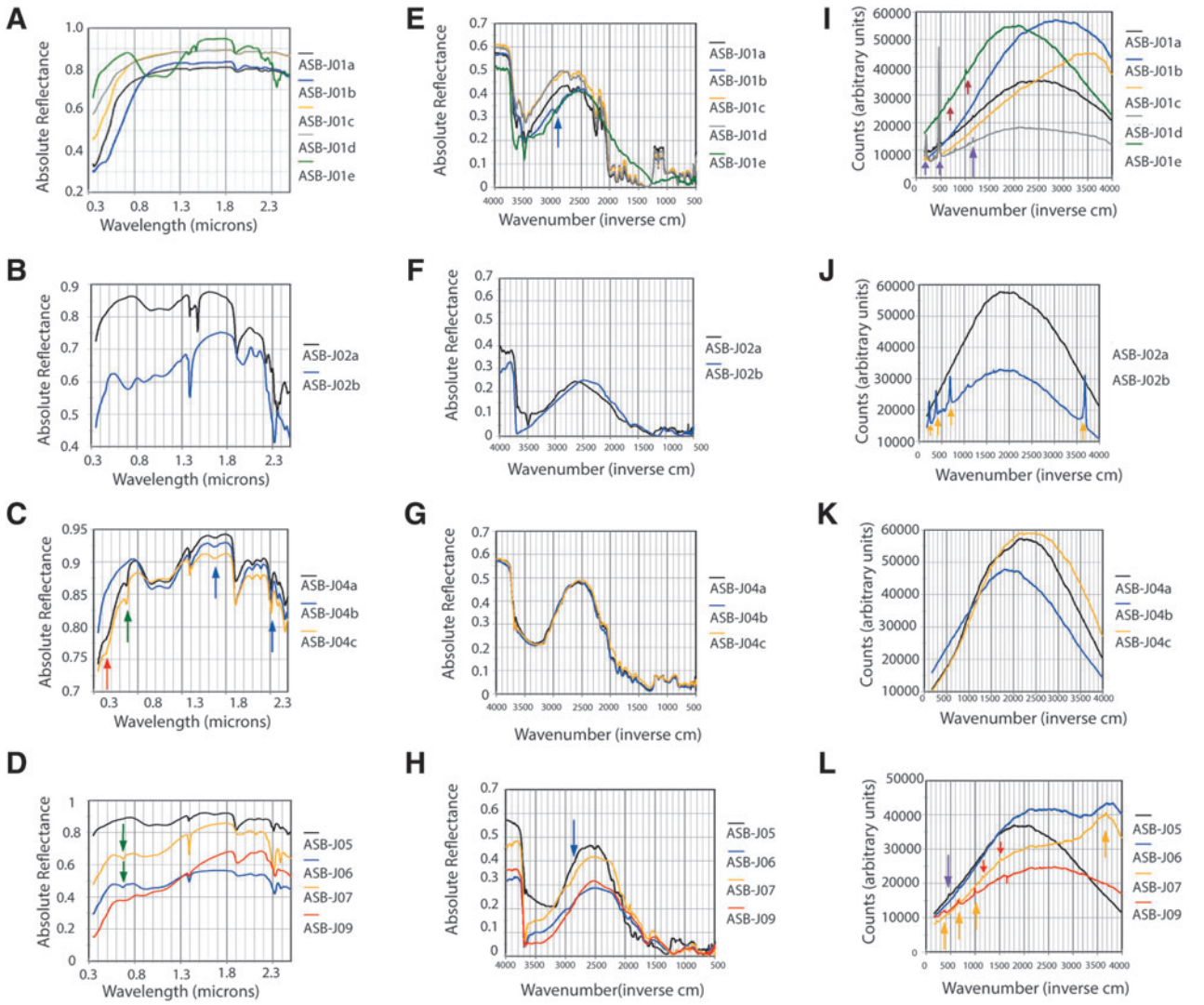

FIG. 3. Reflectance and Raman spectra of samples. **(A–D)** 0.35–2.5 μm reflectance spectra of the samples: **(A)** ASB-J01a-e; **(B)** ASB-J02a-b; **(C)** ASB-J04a-c; **(D)** ASB-J05, J06, J07, and J09. **(E–H)** 2.5–20 μm (4000–500 cm^{-1}) reflectance spectra of the samples: **(E)** ASB-J01a–e; **(F)** ASB-J02a–b; **(G)** ASB-J04a–c; **(H)** ASB-J05, J06, J07, and J09. **(I–L)** Raman reflectance spectra (174–4000 cm^{-1}): **(I)** ASB-J01a–e; **(J)** ASB-J02a–b; **(K)** ASB-J04a–c; **(L)** ASB-J05, J06, J07, and J09. Arrows indicate various absorption features of interest. Red arrows indicate the carotenoid-associated absorption band. Green arrows denote chlorophyll-associated absorption band, blue arrows indicate aliphatic C-H-associated absorption bands, violet arrows indicate quartz, brown arrows indicate diopside, and orange arrows indicate serpentine.

attributable to OH/H_2O (Clark *et al.*, 1990), and minor bands beyond 2.2 μm that are likely due to trace amounts of various metal-bearing hydrated components. The spectrum of ASB-J01d and e shows two absorption bands in the 0.9–1.2 μm region (near 0.95 and 1.15 μm) attributable to ferrous iron in diopside (Cloutis and Gaffey, 1991), whereas the longer wavelength bands are largely attributable to OH/H_2O (1.4 and 1.9 μm regions) and phyllosilicates, such as sericite.

Two subsamples of ASB-J02 (a and b) (Fig. 3B) show absorption bands largely attributable to their mineralogy as determined by XRD. The ASB-J02a spectrum has absorption bands attributable to Fe^{2+} near 0.95 and 1.15 μm likely due to minor diopside (which was not detected by XRD) and absorption bands in the 1.4, 1.9, and >2.2 μm regions due to OH/H_2O and various hydrated silicates (Clark *et al.*, 1990). The spectrum of ASB-J02b shows absorption bands characteristic of serpentine: an Fe^{2+}–Fe^{3+} charge transfer band near 0.70 μm, Fe^{2+} crystal field transitions near 0.9 and 1.1 μm, a sharp OH stretching overtone band near 1.39, and a metal–OH combination band near 2.32 μm (Clark *et al.*, 1990). The assignments of the broad band at 1.9–2.0 μm and band at 2.1 μm are not yet known. Despite the visual identification of endoliths in ASB-J02a, there is no strong evidence for carotenoid or chlorophyll absorption bands.

Two of the ASB-J04 spectra (ASB-J04a, ASB-J04c; Fig. 3C) show clear evidence of carotenoid (red arrow) and chlorophyll (green arrow) absorption features, near 0.45 and 0.67 μm, respectively. The endoliths likely also account for the aliphatic C-H stretching and bending overtone and combination bands near 1.67 and 2.31 μm (blue arrows

in Fig. 3C). All three spectra show evidence of diopside (absorption bands near 0.95 and 1.15 μm) and hydrated silicates (bands in the 1.4 and 1.9 μm regions). Spectroscopic detections of minor phases (*i.e.*, diopside) that are not evident in XRD are possible when the minor phases are present in a transparent medium (quartz and albite in this case).

Reflectance spectra of ASB-J05 (quartzofeldspathic), ASB-J06 and J07 (serpentinite), and ASB-J09 (vermiculitic) are shown in Figure 3D. The ASB-J06 and J07 spectra show the clearest evidence for endoliths—both display the narrow chlorophyll absorption band at 0.67 μm. The carotenoid and aliphatic C-H bands are not seen (expected at 0.45, 1.67, and 2.31 μm). The latter may be present but obscured by serpentine/hydrated silicate absorption bands in this region. All the spectra show Fe^{2+}-associated absorption bands in the 0.9 and 1.1 μm regions. Note that band positions are similar for diopside (likely present in ASB-J05), serpentine (present in ASB-J06 and J07), and amphibole (present in ASB-J09).

3.3. IR 2.5–20 μm (4000–500 cm^{-1}) reflectance spectra

IR (2.5–20 μm; 4000–500 cm^{-1}) reflectance spectra of the ASB-J01 samples are shown in Figure 3E. They are characterized by a region of moderate absorption between ~3700 and 2700 cm^{-1}. This region includes absorption bands due to OH (~3700 cm^{-1}), H_2O (~3300 cm^{-1}), and aliphatic C-H (~2900 cm^{-1}). Interestingly, aliphatic C-H fundamental stretching bands appear in at least three of these spectra, suggesting that this wavelength region may be more sensitive than the 0.67 μm region for endolith detection. Differences in this wavelength region between ASB-J01e and the others are apparent in terms of relative absorption band depths, such as the OH band near 3700 cm^{-1}. At longer wavelengths, major differences exist in the 2200 and 1100 cm^{-1} regions, where quartz has strong and diagnostic spectral features, which are highly suppressed in the quartz-poor ASB-J01e spectrum.

Spectral differences in the IR also exist between the two ASB-J02 samples (Fig. 3F). The serpentine-rich sample (ASB-J02b) shows a stronger OH absorption band at 3700 cm^{-1}. Differences in the silicates also appear as differences in positions of longer wavelength Si-O stretching and bending absorption bands.

The ASB-J04 IR spectra (Fig. 3G) are nearly identical to each other, with absorption bands attributable to OH/H_2O (3100–3700 cm^{-1}), H_2O (1600 cm^{-1}), and Si/Al-O (900–2200 cm^{-1}). Interestingly, even though two of the visible region spectra (Fig. 3C: ASB-J04a, c) show a chlorophyll absorption feature near 0.67 μm, organic absorption bands are not apparent in the IR spectra, likely being masked by the H_2O absorption feature.

In contrast to the ASB-J04 spectra, ASB-J06 and ASB-J07, which both showed a chlorophyll absorption band near 0.67 μm (Fig. 3D), also show CH aliphatic bands near 2900 cm^{-1} (Fig. 3H). Also, as seen in previous spectra, the quartz-dominated assemblages show the distinct double-peaked feature in the 1000–1200 cm^{-1} region, along with other differences that distinguish serpentine from quartz-dominated assemblages.

3.4. Raman spectra

Raman spectra of the samples generally show few well-defined Raman peaks (Fig. 3I–L), due to strong fluorescence, which may be biotic or abiotic (Cloutis *et al.*, 2011; Rhind *et al.*, 2014). Raman spectra of the ASB-J01 spectra show few Raman peaks (Fig. 3I). They are most prominent in the ASB-J01a, c, and d spectra, and the major peaks are attributable to quartz, consistent with the XRD results indicating major quartz in these samples. The ASB-J01e spectrum is dominated by diopside peaks, consistent with XRD and reflectance data. The ASB-J01d spectrum exhibits a peak near 1090 cm^{-1} that is probably due to dolomite. Some of the spectra have additional minor peaks whose identity is uncertain, but which are not consistent with carotenoids or chlorophyll. The ASB-J02 spectra continue the trend of being spectrally different (Fig. 3J). The ASB-J02a spectrum has a fluorescence hump and no Raman peaks, whereas the ASB-J02b spectrum has a number of peaks, all attributable to serpentine, including an OH stretching peak near 3700 cm^{-1} (Andreani *et al.*, 2008).

The ASB-J04 Raman spectra are all devoid of well-defined Raman peaks (Fig. 3K), but do show differences in their fluorescence profiles. The ASB-J05, 06, 07, and 09 Raman spectra show differences in the number of Raman peaks and their positions (Fig. 3L). The ASB-J05 spectrum shows one resolvable Raman peak attributable to Si-O bending modes in quartz (near 460 cm^{-1}). The ASB-J06 spectrum also shows at least one peak, attributable to serpentine (near 680 cm^{-1}), as well as a hump in the 3700 cm^{-1} region that is consistent with serpentine. The ASB-J07 spectrum has one peak that can be attributed to quartz, as well as two peaks attributable to carotenoids near 1150 and 1500 cm^{-1} (but no chlorophyll-associated peaks). The fluorescence hump centered near ~3800 cm^{-1} seen in ASB-J01b, ASB-J06, and ASB-J07 is likely due to chlorophyll. The ASB-J09 Raman spectrum has more peaks than the others, but is generally consistent with a serpentine-dominant mineralogy. The 300–400 cm^{-1} features are ascribable to Si-O bending modes; the ~680 cm^{-1} band is ascribable to Si-O asymmetric stretching modes; and the ~1000 cm^{-1} band is ascribable to Si-O asymmetric stretching modes. The presence of chlorophyll and carotenoids in both quartzofeldspathic and serpentinite samples suggests that at least a component of these lithic microbial communities derives energy by photosynthesis.

3.5. Scanning electron microscopy

Scanning electron microscopy showed the presence of microorganisms consistent in size with both bacterial and eukaryotic cells in all quartzofeldspathic intrusive endolithic habitats (Fig. 4). Bacterial cells were observed adhering to the rock surface through fimbriae attachment in quartzofeldspathic samples 1 and 3 (Fig. 4A, E). Serpentinite fibers and fungal hyphae were only imaged in quartzofeldspathic sample 2 (Fig. 4B). Eukaryotic-sized microorganisms were more abundant in quartzofeldspathic samples 3 and 4 than in the other two samples (Fig. 4C–G). Dividing cells were also observed (Fig. 4D). Although the presence of microorganisms was difficult to confirm by SEM in serpentinite samples, several large microaggregates were observed within antigorite matrices (Fig. 4H) that could host microbial communities (Fig. 4I–L).

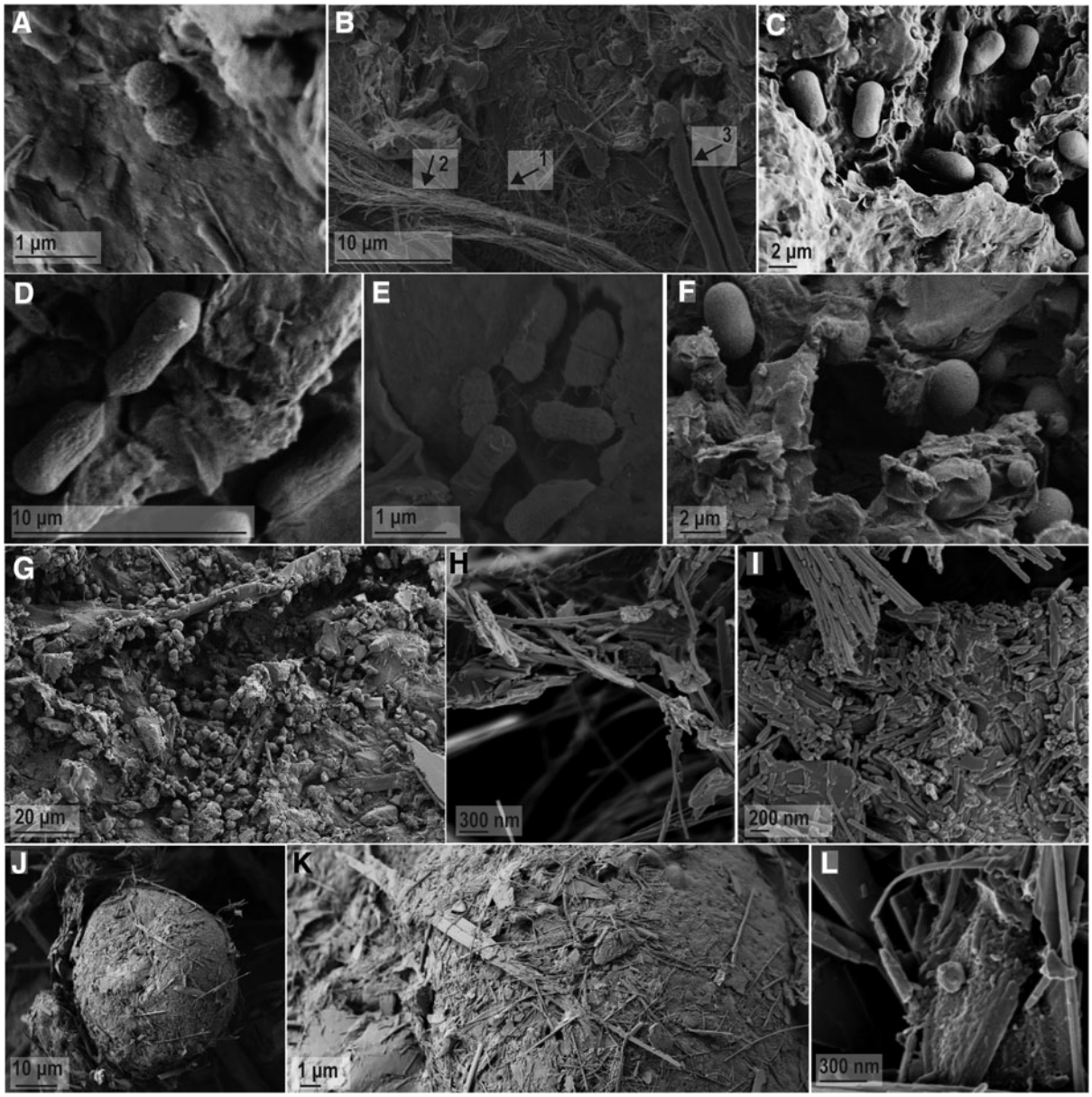

FIG. 4. Representative SEM secondary electron images of lithic communities. **(A)** Two cells consistent with bacterial size located on the surface of the quartzofeldspathic sample ASB-J01. **(B)** Three bacterial cells are visible in the quartzofeldspathic sample ASB-J02, as indicated by arrow 1. Fibrous antigorite is visible on the surface of this quartzofeldspathic intrusive, indicated by arrow 2, beside fungal hyphae, indicated by arrow 3. **(C)** Quartzofeldspathic sample ASB-J04 contained cells consistent with the size and shape of eukaryotic cells that could be fungal spores or algae cells. **(D)** These eukaryotic cells were observed during cell division. **(E)** Cells that were a size consistent with bacteria were also present on the surface of sample ASB-J05 and appeared to be associated with the rock surface through small fibers. **(F)** Cells consistent in size with both prokaryotic and eukaryotic cells are viewed in close association with feldspar/quartz sample ASB-J04. **(G)** The abundance of cells was also very high in sample ASB-J04 in comparison with the other samples, which is seen by a lower magnification photo. Textural features consistent with microaggregate fungi are also present in this image. **(H)** Antigorite fibers are prominent in serpentinite sample ASB-J06, and can be, as in **(I–K)**, present in association with a microaggregate that, based on biological activity (radio respiration assays) and the presence of DNA, likely contains bacteria, fungi, and photosynthetic microorganisms. **(L)** Antigorite fibers are less common in serpentinite sample ASB-J07, and the microaggregates are also present and likely conceal the biological portion of these samples. SEM, scanning electron microscope.

3.6. Heterotrophic activity

Radiolabeled ^{14}C-acetate mineralization assays were used to examine the metabolic potential of the microbial communities hosted in quartzofeldspathic and serpentinite lithologies and at both 24°C and −5°C. At 24°C, both quartzofeldspathic and serpentinite communities demonstrated heterotrophic activity, indicative of a viable heterotrophic population (Fig. 5A, B). At −5°C, the serpentinite community showed heterotrophic activity, but the quartzofeldspathic community did not (Fig. 5C, D).

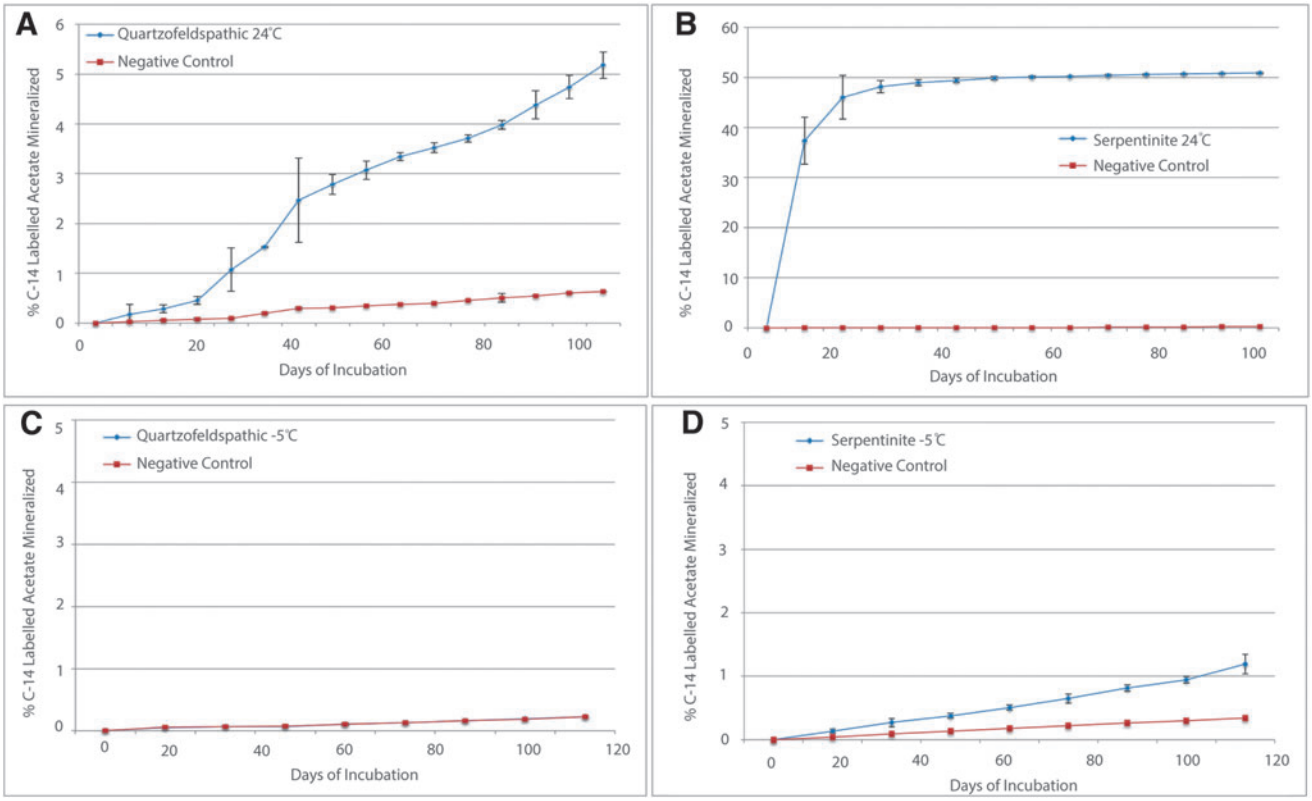

FIG. 5. Radio respiration assays of quartzofeldspathic- and serpentinite-hosted lithic communities. ^{14}C radiolabeled acetate was used to investigate the heterotopic activity of each community at each of the two different temperatures (24°C and −5°C). Both **(A)** quartzofeldspathic and **(B)** serpentinite microbial communities were active at 24°C. **(C)** Quartzofeldspathic communities did not show activity at −5°C, whereas **(D)** serpentinite samples showed some activity, indicating this community may be active for at least part of the winter season, and that serpentinite could potentially host life at temperatures relevant to Mars.

3.7. Microbial community structure

Bacterial 16S rRNA, fungal ITS, and 23 LSU plastid DNA-targeted amplicon sequencing was carried out on each sample. Despite multiple attempts, we were unsuccessful in obtaining archaeal amplicons, suggesting archaea are either low in abundance or absent in these lithic substrates. Before filtering, there were 10,346 bacterial sequences, 15,075 plastid sequences, and 4698 fungal sequences. After filtering for quality, we analyzed 8573 bacterial sequences, 4386 fungal sequences, and 9257 plastid sequences that were classified into OTUs that were defined at a cutoff level of 97% sequence identity. The resultant data were used to calculate diversity indices (Table 2). Using the unpaired *t*-test to evaluate significant differences in diversity or richness, differences were not observed between microbial communities hosted between quartzofeldspathic intrusive or serpentinite ($p > 0.05$), with the exception of Chao richness for the bacterial/agal community. In this comparison, serpentinite samples were shown to have a significantly richer community than the quartzofeldspathic community ($p = 0.0154$).

Major phyla identified from single samples at the phylum level are shown in Figure 6. The 16S rRNA, ITS, and 23 LSU plastid genes were used as a proxy for relative abundance of bacterial, fungal, and photosynthetic plastid-bearing microbial phylotypes, respectively; however, it must be acknowledged that this is a semiquantitative measurement, due to potential DNA isolation and amplification biases. Phyla that dominated the quartzofeldspathic samples tended to also be dominant in the serpentinite samples (Proteobacteria, Cyanobacteria, and Actinobacteria) (Fig. 6A). However, some differences were observed: *Deinococcus-Thermus* and Bacteroidetes were common in the quartzofeldspathic samples but were rare in the serpentinite samples, whereas Planctomycetes were common in serpentinite and rare in quartzofeldspathic samples.

The dominant bacterial OTUs that were also responsible for significant ($p < 0.05$) shifts of samples along the nonmetric multidimentional scaling (NMDS) axes (Fig. 7A) were examined on a finer phylogenic scale by comparing a representative FASTA sequence with the NCBI database using the BLASTn algorithm. Four of these OTUs, found dominantly in quartzofeldspathic samples, were most closely related to *Deinococcus* sp. sequenced from an epilithic biofilm from Spain and France (Ragon *et al.*, 2012), Sonoran Desert soil (Rainey *et al.*, 2005), and glacial melt waters in China. Several additional bacterial OTUs found dominantly in quartzofeldspathic samples were related to uncultured clones or DNA sequenced from hypoliths, other solid surfaces, or endoliths (Pointing *et al.*, 2010). The finding that these sequences most closely resembled, in many instances, sequences from geographically distant soil,

Table 2. Diversity Indices of Lithic Communities from Jeffrey Mine

	Quartzofeldspathic endoliths				*Serpentinite lithic communities*	
Sample	*ASB-J01*	*ASB-J02*	*ADB-J04*	*ASB-J05*	*ASB-J06*	*ASB-J07*
Bacteria						
Good's coverage, %	88	92	90	92	93	82
Number of OTUs (97% cutoff)	126	99	100	99	89	166
Chao richness	515	341	475	327	305	816
Inverse-Simpson	40	20	37	32	11	54
Fungi						
Good's coverage	77	66	83	78	79	74
Number of OTUs (97% cutoff)	51	84	65	81	75	71
Chao richness	596	822	496	432	508	475
Inverse-Simpson	14	23	4	11	14	16
Bacteria/algae						
Good's coverage	95	96	95	96	94	89
Number of OTUs (97% cutoff)	68	59	39	53	44	86
Chao richness	246	182	269	196	347	440
Inverse-Simpson	7	12	3	12	3	14

OTU = operational taxonomic unit.

hypoliths, and endoliths may indicate a unique niche for these phylotypes.

Within the photosynthetic microorganism data set, 20 OTUs were mostly responsible for shifts of samples along the NMDS axis (Fig. 7B), of which 3 were closely related to an uncultured *Chroococcidiopsis* sp. sequence from desert quartz in the Canadian Arctic (Bahl *et al.*, 2011), and 4 OTUs that were more common in quartzofeldspathic intrusive were related to uncultured *Leptolyngbya* sp.

Several fungal species closely related to the Jeffrey Mine sequences in the NCBI database were sequenced from various environmental samples in North America, Canada, and even Québec, none of which were associated with rocks. Fungal communities were dominated by Ascomycota (Fig. 6B) in all minerals. For photoautotrophs, all samples were dominated by Cyanobacteria (Fig. 6C).

4. Discussion

Lithic microorganisms inhabit a unique niche where community composition is influenced by biogeographic factors (climate, water availability, nutrients, and light) and microenvironmental parameters (rock chemistry, texture, and mineralogy). Serpentine is present in a few regions on Mars, including some future rover landing sites (*e.g.*, Jezero crater) (Ehlmann *et al.*, 2010). Although quartzofeldspathic materials are not a focus of Mars exploration, such terrains are present in a number of regions on Mars (Christensen *et al.*, 2005), and silica-rich materials have been detected at Mars Exploration Rover and Mars Science Laboratory landing sites (Ruff *et al.*, 2011; Thompson *et al.*, 2015; Morris *et al.*, 2016). Thus, both major lithologies examined here are relevant to current and future Mars surface exploration efforts. In this study, the Jeffrey Mine was used as a Mars analogue because of the common presence of serpentinite, and we have demonstrated that both quartzofeldspathic and serpentinite rock samples collected from the Jeffrey Mine pit host viable microbial communities *in situ* and that antigorite can support a viable bacterial community to at least −5°C.

Overall, we found that bacteria in our samples were closely related to other bacteria in similar environments from distant geographic locations, whereas the eukaryotic fungi were most closely related to other samples from different environments but from geographically close samples. The fungal communities were dominated by Ascomycota in both of the minerals—and Ascomycota is often found in endolithic communities (Ziolkowski *et al.*, 2013; Goordial *et al.*, 2016). However, Ascomycota sequences were not similar to other endolithic Ascomycota sequences. This may indicate geography is more influential than lithology in determining eukaryotic community structure, a hypothesis that has been proposed by Ragon *et al.* (2012), whereas lithology is more important for prokaryotes. Explanations for this observation could be related to dispersal and survivability of prokaryotic versus eukaryotic microorganisms; dominant bacterial groups in our samples clustered to clades that tend to be resistant to desiccation and ultraviolet and ionizing radiation, which would lead to their stochastic success, colonizing lithic niches by dust particle dispersal over wide geographic areas (Brodie *et al.*, 2007; Ragon *et al.*, 2012).

The spectral results presented here demonstrate the complementarity of different spectroscopic techniques for investigating the geology and biology of samples. Reflectance spectroscopy in the <2.5 μm region appears to be best suited for detecting endoliths on the basis of a diagnostic chlorophyll absorption band near 0.67 μm, as well as carotenoids and aliphatic CH molecules in some cases, although endolith-related features are also seen in IR and Raman spectra. Interestingly, and for reasons not yet understood, not all techniques detected organics/endoliths in the same samples. The <2.5 μm reflectance spectra are very sensitive to optically active atoms such as Fe in different oxidation states, as well as OH/H_2O, and metal–OH absorption bands. The >2.5 μm region is also sensitive to OH/H_2O, as well as framework type molecules such as Si-O, but not able to directly detect Fe or determine its

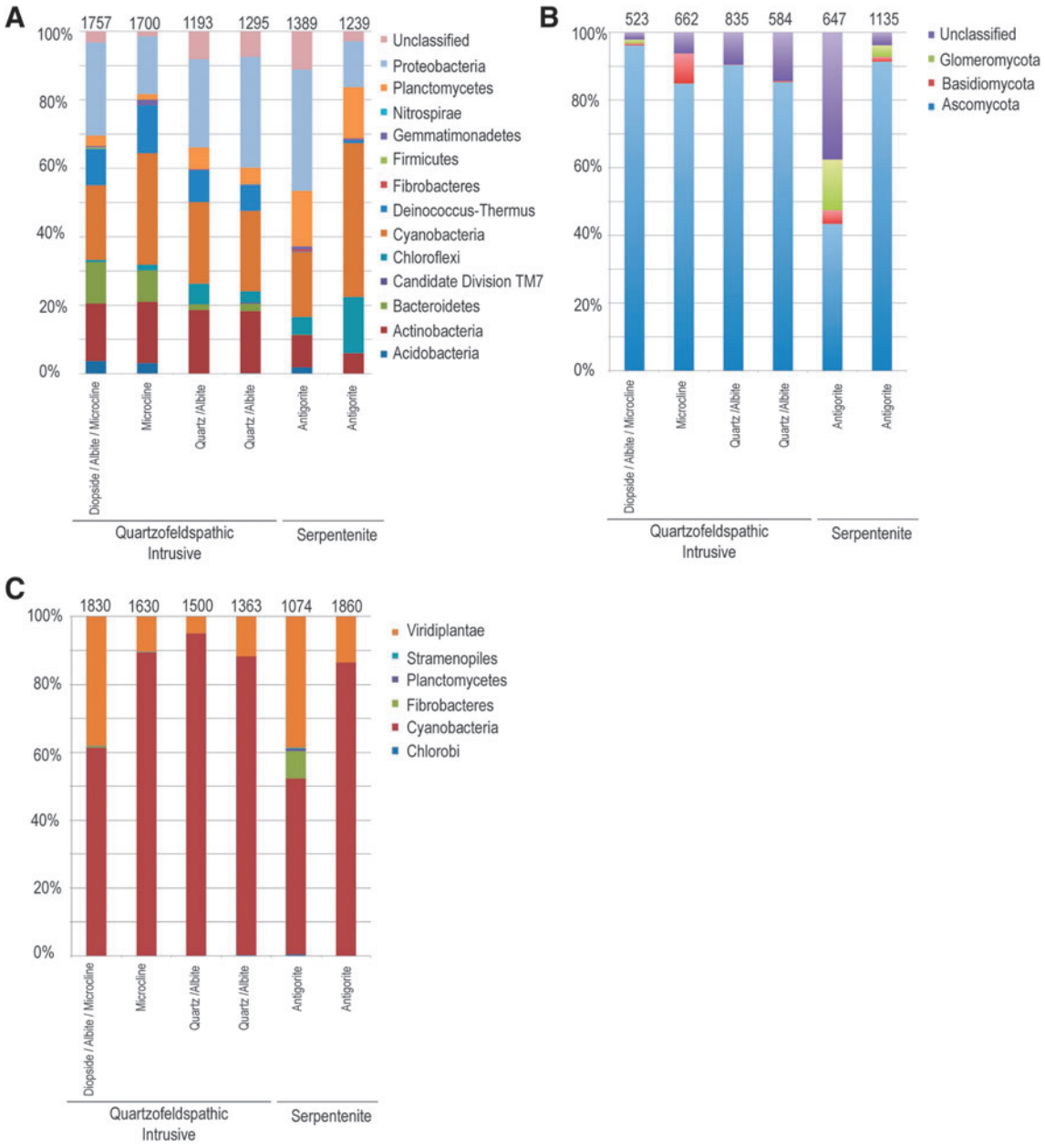

FIG. 6. Bar graphs indicating composition of microbial communities for single samples ($n = 1$). **(A)** The composition of the bacterial communities of each sample is displayed at the phylum level. The phyla Dinococcus-Thermus and Bacteroidetes are noticeably present in quartzofeldspathic intrusive samples, although absent from serpentinite-hosted communities. **(B)** Fungal community composition is shown at the phyla level. Ascomycota dominated each sample, although Basidiomcyota was present in each sample as well. **(C)** The photoautotrophic community is displayed to the phylum level. The number of sequences present in each sample, used to construct the charts, is displayed at the top of each column.

oxidation state. Raman spectra may be featureless or exhibit only one or a few bands. Because many minerals and organic molecules may have Raman peaks in similar positions, when only a few Raman peaks are present, unique assignments may not be possible. However, it appears that it can detect the presence of endoliths in at least one of the samples through carotenoid Raman peaks.

Evaluation of the quartzofeldspathic samples by SEM showed that endolithic microbial communities consist of both bacterial and eukaryotic cells in close association with mineral surfaces. Microorganisms in the antigorite sample were much more difficult to image; although microaggregates were prominent in samples (Fig. 4H–K), no clear cellular structures were observed. However, abundant corroborative evidence confirms their presence including ample DNA, spectral signatures of chlorophyll, and high levels of heterotrophic activity relative to the quartzofeldspathic intrusive population.

Microbial communities hosted in the serpentinite at Jeffrey Mine displayed more heterotrophic activity at 24°C than did

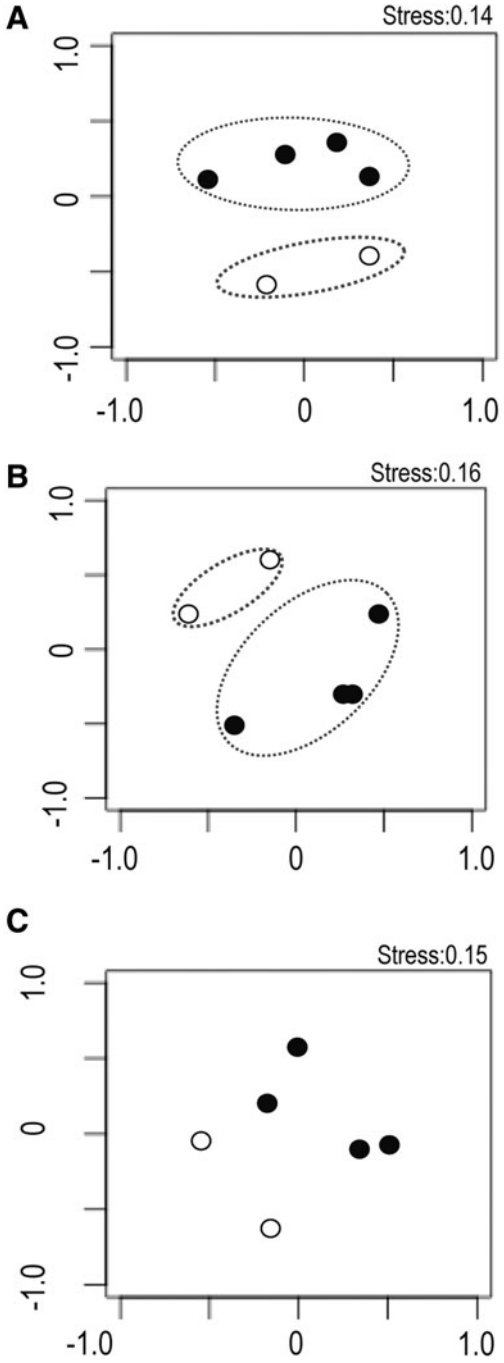

FIG. 7. Comparison of **(A)** bacterial, **(B)** bacterial/algal, and **(C)** fungal communities on the basis of sample mineralogy. Quartzofeldspathic intrusive hosted communities are denoted by filled black circles, whereas communities hosted in serpentenite are shown by white circles. Community relatedness is displayed by NMDS. Sequence distance was calculated based on clustering OTUs at a 0.03 cutoff and subsampling each of the data sets to 1196, 529, and 1135 sequences for bacteria, fungi, and bacterial/algal communities, respectively. The dashed lines represent statistically significant groupings based on Analysis of MOlecular VAriance (AMOVA), where $p < 0.1$ and $n = 6$. The fungal community did not show any statically significant community groupings ($p = 0.135$), however, in bacterial ($p = 0.011$) and bacterial/algal ($p = 0.067$), significant phylogeny groupings corresponded with the mineralogy of the samples. NMDS, nonmetric multidimensional scaling. OTUs, operational taxonomic units.

quartzofeldspathic communities, and maintained detectable metabolic activity in cryophilic conditions (−5°C), where the quartzofeldspathic communities were inactive at −5°C. The reasons for the difference in temperature adaptation in the two rock types are unclear; however, it suggests that the serpentenite lithology may host microbial communities that are better able to adapt to cold temperatures. Serpentinite at Jeffrey Mine has high chemical diversity, relative to the quartzofeldspathic intrusive, particularly with respect to biologically significant transition metals. Transition metals function as the catalytic centers of enzyme catalysts, and their presence is absolutely essential for cell functioning (Wackett *et al.*, 2004; Gadd, 2010). Serpentinites are rich in transition metals including manganese, iron, nickel, and zinc, whereas quartzofeldspathic rocks are generally lower in transition metals. It is possible that the observed high metabolic activity observed in the serpentinite samples, relative to the quartzofeldspathic sample, may have been a result of the microorganisms in the quartzofeldspathic sample being starved for transition metals; however, this is only speculation.

If the active microbial communities in the serpentinites are indeed utilizing transition metals either in redox-based chemoautolithic metabolic reactions or as coenzymes and cofactor incorporated into organometallo complexes through catalysis, these patterns have the potential to be preserved as geochemical biosignatures in the serpentine. The biologically mediated transformation of redox states of transition metals can be preserved as a potential indicator of metabolic activity, whereas scavenging of transition metals for biological incorporation may be preserved as conspicuous depletion patterns.

Lithic habitats have been proposed as promising sites for the detection of ancient life or remnant biosignatures on the surface of Mars, with determination of which lithologies to direct precious resources toward investigating of critical concern. When life arose on Earth ~3.8 Gyr ago, environmental conditions on Mars were probably similar to those on the early Earth (Davis and McKay, 1996; McKay, 1997; Holm and Andersson, 2005) and may have allowed martian life to have independently arisen. On modern Mars, living organisms and organic compounds exposed to the unfiltered solar radiation and oxidizing surface conditions are rapidly destroyed or altered (Stoker and Bullock, 1997). Had life existed on ancient Mars, these organisms may have taken refuge in lithic environments in a manner similar to microorganisms in extreme terrestrial environments (McKay *et al.*, 1996; McKay, 1997). Terrestrial lithic niches are, therefore, of astrobiological interest, particularly if they occur in lithologies that are relevant to Mars. Our finding that terrestrial surficial serpentinites associated with methane emissions host diverse and viable microbial communities on Earth makes them a potential analogue for interpreting observations on Mars (Ehlmann *et al.*, 2010); this indicates martian serpentinites warrant further study with a focus on exobiology. In addition, since the martian climate is considerably colder than Earth's, the finding that serpentinite-hosted communities remain viable and metabolically active down to at least −5°C makes this proposal even more significant.

Acknowledgments

The University of Winnipeg's HOSERLab was established with funding from the Canada Foundation for Innovation, the Manitoba Research Innovations Fund, and the Canadian Space Agency, whose support is gratefully acknowledged. This study was supported by research grants from NSERC, the Canadian Space Agency, and the University of Winnipeg. J.R., J.G., H.M.S., A.P., G.L.G., and M.R.M.I. gratefully acknowledge funding from the NSERC CREATE Canadian Astrobiology Training Program. M.R.M.I. also thanks the Mineralogical Association of Canada.

Author Disclosure Statement

No competing financial interests exist.

References

Andreani, M., Grauby, O., Baronnet, A., and Munoz, M. (2008) Occurrence, composition, and growth of polyhedral serpentine. *European J Mineral* 20:159–172.

Bahl, J., Lau, M.C.Y., Smith, G.J.D., Vijaykrishna, D., Cary, S.C., Lacap, D.C., Lee, C.K., Papke, R.T., Warren-Rhodes, K.A., Wong, F.K.Y., McKay, C.P., and Pointing, S.B. (2011) Ancient origins determine global biogeography of hot and cold desert cyanobacteria. *Nat Commun* 2:161–166.

Bell, T.H., Hassan, S.E-D., Lauron-Moreau, A.E.L., Al-Otaibi, F., Hijri, M., Yergeau, E., and St-Arnaud, M. (2013) Linkage between bacterial and fungal rhizosphere communities in hydrocarbon-contaminated soils is related to plant phylogeny. *ISME J*. 8:331–343.

Blamey, N.J.F., Pharnell, J., McMahon, S., Mark, D.F., Tomkinson, T., Lee, M., Shivak, J., Izawa, M.R.M., Banerjee, N.R., and Flemming, R.L. (2015) Evidence for methane in Martian meteorites. *Nat Commun* 6:7399.

Brazelton, W.J., Thornton, C.N., Hyer, A., Twing, K.I., Longino, A.A., Lang, S.Q., Lilley, M.D., Früh-Green, G.L., and Schrenk, M.O. (2017) Metagenomic identification of active methanogens and methanotrophs in serpentinite springs of the Voltri Massif, Italy. *PeerJ* 5:e2945.

Brodie, E.L., DeSantis, T.Z., Parker, J.P.M., Zubietta, I.X., Piceno, Y.M., and Andersen, G.L. (2007) Urban aerosols harbor diverse and dynamic bacterial populations. *Proc Natl Acad Sci U S A* 104:299–304.

Caruso, T., Chan, Y., Lacap, D.C., Lau, M.C.Y., McKay, C.P., and Pointing, S.B. (2011) Stochastic and deterministic processes interact in the assembly of desert microbial communities on a global scale. *ISME J* 5:1406–1413.

Christensen, P.R., McSween, H.Y., Bandfield, J.L., Ruff, S.W., Rogers, A.D., Hamilton,V.E., Gorelick, N., Wyatt, M.B., Jakosky, B.M., Kieffer, H.H., Malin, M.C., and Moersch, J.E. (2005) Evidence for magmatic evolution and diversity of Mars from infrared observations. *Nature* 436: 504–509.

Clark, R.N., King, T.V.V., Klewja, M., Swayze, G.A., and Vergo, N. (1990) High spectral resolution reflectance spectroscopy of minerals. *J Geophys Res* 95:12653–12680.

Cloutis, E.A., and Gaffey, M.J. (1991) Pyroxene spectroscopy revisited: Spectral–compositional correlations and relationship to geothermometry. *J Geophys Res Planets* 96:22809–22826.

Cloutis, E.A., Hiroi, T., Gaffey, M.J., Alexander, C.M.O., and Mann, P. (2011) Spectral reflectance properties of carbonaceous chondrites: 1. CI chondrites. *Icarus* 212: 180–209.

Davila, A.F., Gómez-Silva, B., de los Rios, A., Ascaso, C., Olivares, H., McKay, C.P., and Wierzchos, J. (2008) Facilitation of endolithic microbial survival in the hyperarid core of the Atacama Desert by mineral deliquescence. *J Geophys Res* 113:G01028.

Davis, W.L. and McKay, C.P. (1996) Origins of life: a comparison of theories and application to Mars. *Orig Life Evol Biosph* 26:61–73.

Ehlmann, B.L. and Mustard, J.F. (2012) An in-situ record of major environmental transitions on early Mars at Northeast Syrtis Major. *Geophys Res Lett* 39, doi:10.1029/2012 GL051594.

Ehlmann, B.L., Mustard, J.F., and Murchie, S.L. (2010) Geologic setting of serpentine deposits on Mars. *Geophys Res Lett* 37, doi:10.1029/2010GL042596.

Evans, B.W. (2004) The serpentinite multisystem revisited: chrysotile is metastable. *Int Geol Rev* 46:479–506.

Gadd, G.M. (2010) Metals, minerals and microbes: geomicrobiology and bioremediation. *Microbiology* 156:609–643.

Good, I.J. (1953) The Population Frequencies of Species and the Estimation of Population Parameters. *Biometrika* 40: 237–264.

Goordial, J., Davila, A., Lacelle, D., Pollard, W., Marinova, M.M., Greer, C.W., DiRuggiero, J., McKay, C.P., and Whyte, L.G. (2016) Nearing the cold-arid limits of microbial life in permafrost of an upper dry valley, Antarctica. *ISME J* 10: 1613–1624.

Hayat, M.A. (2000) *Principles and Techniques of Electron Microscopy: Biological Applications*, 4th ed., Cambridge University Press, Cambridge.

Holm, N.G. and Andersson, E. (2005) Hydrothermal simulation experiments as a tool for studies of the origin of life on Earth and other terrestrial planets: a review. *Astrobiology* 5:444–460.

Huson, D.H., Auch, A.F., Qi, J., and Schuster, S.C. (2007) MEGAN analysis of metagenomic data. *Genome Res* 17:377–386.

Jørgensen, S.L. and Zhao, R. (2016) Microbial inventory of deeply buried oceanic crust from a young ridge flank. Front Microbiol 7:820.

Lang, S.Q., Früh-Green, G.L., Bernasconi, S.M., Lilley, M.D., Proskurowski, G., Méhay, S., and Butterfield, D.A. (2012) Microbial utilization of abiogenic carbon and hydrogen in a serpentinite-hosted system. *Geochim Cosmochim Acta* 92: 82–99.

Laurent, R. and Hébert, Y. (1979) Paragenesis of serpentine assemblages in harzburgite tectonite and dunite cumulate from the Quebec Appalachians. *Can Mineral* 17:857–869.

Lee, M.D., Walworth, N.G., and Sylvan, J.B. (2015) Microbial communities on seafloor basalts at Dorado Outcrop reflect level of alteration and highlight global lithic clades. *Front Microbiol* 6:403.

Marlow, J.J., LaRowe, D.E., Ehlmann, B.L., Amend, J.P., and Orphan, V.J. (2014) The potential for biologically catalyzed anaerobic methane oxidation on ancient Mars. *Astrobiology* 4:292–307.

McFrederick, Q.S., Cannone, J.J., Gutell, R.R., Kellner, K., Plowes, R.M., Mueller, and U.G. (2013) Specificity be-

tween Lactobacilli and Hymenopteran Hosts Is the Exception Rather than the Rule. *Appl Environ Microbiol* 79: 1803–1812.

McKay, C.P. (1997) The search for life on Mars. *Orig Life Evol Biosph* 27:263–289.

McKay, D.S.D., Gibson, E.K.E., Thomas-Keprta, K.L.K., Vali, H.H., Romanek, C.S.C., Clemett, S.J.S., Chillier, X.D.X., Maechling, C.R.C., and Zare, R.N.R. (1996) Search for past life on Mars: possible relic biogenic activity in martian meteorite ALH84001. *Science* 273:924–930.

Morris, R.V., Vaniman, D.T., Blake, D.F., Gellert, R., Chipera, S.J., Rampe, E.B., Ming, D.W., Morrison, S.M., Downs, R.T., Treiman, A.H., Yen, A.S., Grotzinger, J.P., Achilles, C.N., Bristow, T.F., Crisp, J.A., Des Marais, D.J., Farmer, J.D., Fendrich, K.V., Frydenvang, J., Graff, T.G., Morookian, J.M., Stolper, E.M., and Schwenzer, S.P. (2016) Silicic volcanism on Mars evidenced by tridymite in high-SiO2 sedimentary rock at Gale crater. *Proc Natl Acad Sci U S A* 113:7071–7076.

Mount, D.W. (2007) Using the basic local alignment search tool (BLAST). *Cold Spring Harbor Protoc* 2017:pdb.top17–pdb.top17.

Normand, C. and Williams-Jones, A.E. (2007) Physicochemical conditions and timing of rodingite formation: evidence from rodingite-hosted fluid inclusions in the JM Asbestos mine, Asbestos, Québec. *Geochem Trans* 8:11.

Omelon, C.R., Pollard, W.H., and Ferris, F.G. (2006) Environmental controls on microbial colonization of high Arctic cryptoendolithic habitats. *Polar Biol* 30:19–29.

Omelon, C.R., Pollard, W.H., and Ferris, F.G. (2007) Inorganic species distribution and microbial diversity within high arctic cryptoendolithic habitats. *Microb Ecol* 54:740–752.

Orcutt, B.N., Sylvan, J.B., and Rogers, D. (2015) Carbon fixation by basalt-hosted microbial communities. *Front Microbiol* 6: 301.

Oze, C. and Sharma, M. (2005) Have olivine, will gas: serpentinization and the abiogenic production of methane on Mars. *Geophys Res Lett* 32:1–4.

Pointing, S.B., Chan, Y., Lacap, D.C., and Lau, M. (2010) Highly specialized microbial diversity in hyper-arid polar desert. *Proc Natl Acad Sci U S A* 106:19964–19969.

Qadi, A., Cloutis, E., Samson, C., Whyte, L., Ellery, A., Bell, J.F., III, Berard, G., Boivin, A., Haddad, E., Lavoie, J., Jamroz, W., Kruzelecky, R., Mack, A., Mann, P., Olsen, K., Perrot, M., Popa, D., Rhind, T., Sharma, R., Stromberg, J., Strong, K., Tremblay, A., Wilhelm, R., Wing, B., and Wong, B. (2015) Mars methane analogue mission: mission simulation and rover operations at Jeffrey Mine and Norbestos Mine Quebec, Canada. *Adv Space Res* 55:2414–2426.

Quesnel, Y., Sotin, C., Langlais, B., Costin, S., Mandea, M., Gottschalk, M., and Dyment, J. (2009) Serpentinization of the martian crust during Noachian. *Earth Planet Sci Lett* 277:184–193.

Ragon, M., Fontaine, M.C., Moreira, D., and López-García, P. (2012). Different biogeographic patterns of prokaryotes and microbial eukaryotes in epilithic biofilms. *Mol Ecol* 21: 3852–3868.

Rainey, F.A., Ray, K., Ferreira, M., Gatz, B.Z., Nobre, M.F., Bagaley, D., Rash, B.A., Park, M.J., Earl, A.M., Shank, N.C., Small, A.M., Henk, M.C., Battista, J.R., Kampfer, P., and da Costa, M.S. (2005) Extensive diversity of ionizing-radiation-resistant bacteria recovered from Sonoran desert soil and description of nine new species of the genus *Deinococcus* obtained from a single soil sample. *Appl Environ Microbiol* 71:5225–5235.

Rhind, T., Ronholm, J., Berg, B., Mann, P., Applin, D., Stromberg, J., Sharma, R., Whyte, L.G., and Cloutis, E.A. (2014) Gypsum-hosted endolithic communities of the Lake St. Martin impact structure, Manitoba, Canada: spectroscopic detectability and implications for Mars. *Int J Astrobiol* 13: 366–377.

Ruff, S.W., Farmer, J.D., Calvin, W.M., Herkenhoff, K.E., Johnson, J.R., Morris, R.V., Rice, M.S., Arvidson, R.E., Bell III, J.F., Christensen, P.R., and Squyres, S.W. (2011) Characteristics, distribution, origin, and significance of opaline silica observed by the Spirit rover in Gusev crater, *Mars J Geophys Res* 116:E00F23.

Schloss, P.D., Westcott, S.L., Ryabin, T., Hall, J.R., Hartmann, M., Hollister, E.B., Lesniewski, R.A., Oakley, B.B., Parks, D.H., Robinson, C.J., Sahl, J.W., Stres, B., Thallinger, G.G., Van Horn, D.J., and Weber, C.F. (2009) Introducing mothur: open-source, platform-independent, community-supported software for describing and comparing microbial communities. *Appl Environ Microbiol* 75:7537–7541.

Schloss, P.D., Gevers, D., and Westcott, S.L. (2011) Reducing the effects of PCR amplification and sequencing artifacts on 16S rRNA-based studies. *PLoS One* 6:e27310–e27310.

Schulte, M., Blake, D., Hoehler, T., and McCollom, T. (2006) Serpentinization and its implications for life on the early Earth and Mars. *Astrobiology* 6:364–376.

Serrano-Silva, N., Sarria-Guzm, N.Y., Denodooven, L., and Luna-Guido, M. (2014) Methanogenesis and methanotrophy in soil: a review. *Pedosphere* 24:291–307.

Sherwood, A.R., and Presting, G.G. (2007) Universal primers amplify a 23S rDNA plastid marker in eukaryotic algae and cyanobacteria. *J Phycol* 43:605–608.

Starke, V., Kirshtein, J., Fogel, M.L., and Steele, A. (2013) Microbial community composition and endolith colonization at an Arctic thermal spring are driven by calcite precipitation. *Environ Microbiol Rep* 5:648–649.

Steven, B., Briggs, G., McKay, C.P., Pollard, W.H., Greer, C.W., and Whyte, L.G. (2007) Characterization of the microbial diversity in a permafrost sample from the Canadian high Arctic using culture-dependent and culture-independent methods. *FEMS Microbiol Ecol* 59:513–523.

Stivaletta, N. and Barbieri, R. (2009) Endolithic microorganisms from spring mound evaporite deposits (southern Tunisia). *J Arid Environ* 73:33–39.

Stivaletta, N., Lopez-Garcia, P., and Boihem, L. (2010) Biomarkers of endolithic communities within gypsum crusts (southern Tunisia). *Geomicrobiology* 27:101–110.

Stoker, C.R. and Bullock, M.A. (1997) Organic degradation under simulated Martian conditions. *J Geophys Res* 102: 10881–10888.

Swan, B.K., Ehrhardt, C.J., Reifel, K.M., Moreno, L.I., and Valentine, D.L. (2010) Archaeal and bacterial communities respond differently to environmental gradients in anoxic sediments of a California hypersaline lake, the salton sea. *Appl Environ Microbiol* 76:757–768.

Twing, K.I., Brazelton, W.J., Kubo, M.D.Y., Hyer, A.J., Cardace, D., Hoehler, T.M., McCollom, T.M., and Schrenk, M.O. (2017) Serpentinization-influenced groundwater harbors extremely low diversity microbial communities adapted to high pH. *Front Microbiol* 8:308.

Wackett, L.P., Dodge, A.G., and Ellis, L.B.M. (2004) Microbial genomics and the periodic table. *Appl Environ Microbiol* 70: 647–655.

Walker, J.J. and Pace, N.R. (2007a) Phylogenetic Composition of Rocky Mountain Endolithic Microbial Ecosystems. *Appl Environ Microbiol* 73:3497–3504.

Walker, J.J. and Pace, N.R. (2007b) Endolithic microbial ecosystems. *Annu Rev Microbiol* 61:331–347.

Walker, J.J., Spear, J.R., and Pace, N.R. (2005) Geobiology of a microbial endolithic community in the Yellowstone geothermal environment. *Nature* 434:1011–1014.

Wierzchos, J., Cámara, B., De Los Ríos, A., Davila, A.F., Almazo, I.M.S., Artieda, O., Wierzchos, K., Gómez-Silva, B., McKay, C., and Ascaso, C. (2011) Microbial colonization of Ca-sulfate crusts in the hyperarid core of the Atacama Desert: implications for the search for life on Mars. *Geobiology* 9:44–60.

Wong, F.K.Y., Lau, M.C.Y., Lacap, D.C., Aitchison, J.C., Cowan, D.A., and Pointing, S.B. (2009) Endolithic microbial colonization of limestone in a high-altitude arid environment. *Microb Ecol* 59:689–699.

Wray, J.J. and Ehlmann, B.L. (2011) Geology of possible martian methane source regions. *Planet Space Sci* 59: 196–202.

Ziolkowski, L.A., Mykytczuk, N.C.S., Omelon, C.R., Johnson, H., Whyte, L.G., and Slater, G.F. (2013) Arctic Gypsum Endoliths: a biogeochemical characterization of a viable and active microbial community. *Biogeosci Discuss* 10:2269–2304.

Address correspondence to:
Jennifer Ronholm
Department of Food Science and Agricultural Chemistry
Faculty of Agricultural and Environmental Sciences
Macdonald Campus
McGill University
21,111 Lakeshore
Ste Anne de Bellevue, QC H9X 3V9
Canada

E-mail: Jennifer.Ronholm@mcgill.ca

Submitted 21 April 2017
Accepted 18 January 2018

Abbreviations Used

IR = infrared
ITS = internal transcribed spacer
LCA = Lowest Common Ancestor
LSU = large subunit
MID = multiplex identifier
NMDS = nonmetric multidimensional scaling
OTUs = operational taxonomic units
SEM = scanning electron microscopy
XRD = X-ray diffraction